Electrical characterization of carbon plasma generated by excimer laser ablation of graphite

Petru-Edward Nica, Cristian Ursu, Cristian Focsa

Electrical characterization of carbon plasma generated by excimer laser ablation of graphite

P. Nica[1], C. Ursu[2*], and C. Focsa[3]

[1] *Department of Physics, "Gheorghe Asachi" Technical University, Iasi, 700050, Romania*

[2] *"Petru Poni" Institute of Macromolecular Chemistry, 41 A Gr. Ghica Voda Alley, Iasi 700487, Romania*

[3] *Univ. Lille, CNRS, UMR 8523, PhLAM – Physique des Lasers, Atomes et Molécules, F-59000 Lille, France*

[*]Author for correspondence: cristian.ursu@icmpp.ro

Abstract:

The vacuum expansion of a transient carbon plasma produced by KrF excimer laser at moderate fluences is investigated by separating different types of ions with an electrostatic energy analyzer. In the retarding field of the analyzer, the ion current reveals a multi-peak structure and the signal deconvolution allows obtaining information on the ion abundance and thermal velocity. A significant increase of C^{2+} and C^{1+} fast ions production with the laser pulse energy is observed, while the amount of slower singly charged ions in the thermal plasma part is less affected by the irradiation conditions. By time-integration of the recorded current, the total collected charge *vs.* retarding potential characteristic is built and a derivative method allows obtaining the energy distribution function on the plasma plume axis, in good agreement with the shifted Maxwell-Boltzmann distribution. Future developments of this method are possible through comparison with theoretical fractional ion populations.

Keywords: Excimer laser ablation, carbon plasma dynamics, multicharged ions, electrostatic energy analyzer.

1. Introduction

The ion dynamics in laser-produced plasmas has been a topic of constant interest in the last decades due to various applications, from ion implantation to surface cleaning and patterning or thin film growth by Pulsed Laser Deposition (PLD) [1–3]. Knowing features like energy distribution, average charge state or ion relative abundance allows optimizing various processes in these applications. For example, in the PLD field, the amount of energy carried by the laser-generated ions is of paramount importance for the properties of the grown film. In the particular case of Cr atoms deposited on body-centered cubic CrTi [4], simulations of molecular dynamics showed that kinetic energies lower than 10 eV allow a high mobility of adatoms without defects formation, and thus epitaxy is expected. At about 15 eV, defects appear in the surface layer, while at higher energies re-sputtering of surface atoms occurs, the energetic ions penetrating through a few layers [5] and leading to bulk defect formation. Also, the deposition of energetic ions induces stress and a densification of the deposited material [6,7]. When the PLD technique is employed for the synthesis of diamond-like carbon (DLC) films, kinetic energy of about 90 eV for singly-charged ions allows obtaining maximum content of sp^3-bonded carbon, while above this value the graphitic phase formation was observed [8]. Meantime, a major role is played here by the content of carbon dimer (C_2) in the expanding plasma, which is supposed to influence the formation of large molecules [9–11].

In order to characterize the production of multi-charged ions with pulsed laser beams, the diagnostic systems usually consist in a combination of ion time-of-flight (TOF) measurements, electrostatic mass spectrometer, or ion energy analyzer, allowing to discriminate ions of a certain

charge-to-mass ratio and kinetic energy [12–16]. The TOF signal interpretation is generally based on a shifted Maxwell–Boltzmann (SMB) distribution that can be applied if the ions TOF is much longer than the duration of the driving laser pulse. This distribution involves a thermal velocity (related to the plasma ion temperature) and a "center-of-mass" velocity [17], resulting from collisional processes in the ablation plume. As the expanding plasma generally consists of multiple structures and ions, partial currents must be considered, *i.e.* deconvolution of the total signal must be performed. This is achieved by fixing the value of the maximum charge state and the abundance of each type of ion, parameters that are previously derived with an external electric field used to separate signals from each charge state [16,18]. Following this procedure, in [19] aluminum multi-charged ion generation from femtosecond Ti:sapphire laser ablation is investigated, allowing to demonstrate production of up to Al^{6+} ions, for irradiances in the range of 10^{14} W/cm^2. The ion energy distributions resulted to have two components, a faster one that can be attributed to multiphoton laser ionization, while the slower one is possibly due to collisional processes. Such plume splitting is generally valid for all types of laser ablation, regardless of their temporal regimes, and the mechanisms of laser-plasma interaction are subsequently evidenced into electrostatic and thermal type processes [17,20].

In our previous works [21–23], a new V-shape optical emission from a carbon plasma created by excimer laser ablation of graphite in vacuum was demonstrated. The new shape and the dynamics of plasma were explained by the coexistence and the interaction of three plasmas originating in distinct irradiance areas of the same laser ablation spot. Using various investigation methods (fast-gate ICCD imaging, optical emission spectroscopy, Faraday cup (FC) ion measurements, ablation crater depth profiling) [23], an enhancement of carbon dimer formation was evidenced in an extended spatial region of the plasma. Moreover, a maximum of the ion emission was evidenced along the normal to the target when the angular distribution of the ion

emission was measured with the FC, even though the most visible radiation came from the lateral radiating arms of the V-shape plasma structure. In the frame of a fractal model [24] a theoretical description was also proposed [25]. For a spatial and temporal extension of the optical investigations toward the less emissive axial region of the V-shape carbon plasma, its evolution in an ambient gas was recently studied [26]. Systematic spectroscopic measurements on plasma expansion in Ar gas revealed the influence of collisional processes on the space-time evolution distribution of molecular and atomic species. We observed a wider spreading of carbon dimer relative to the atomic C for longer times and distances. An enhancement of the dimer to atom ratio when going toward lateral radiating arms of plasma was also inferred. Finally, the consistency of the temperature and density evolutions validated the plasma evolution scenario built for this peculiar plume shape [26].

In the present work we bring further insights on the dynamics and energetics of the carbon plasma expanding in vacuum by studying the positively charged particles using an electrostatic energy analyzer (EEA). While in the previous work [23] the focus was on the optical diagnostics (fast-gate ICCD imaging, space-time resolved optical emission spectroscopy) with the aim of explaining the peculiar plasma emission shape, and the electrical characterization (through a simple FC charge collector) was used only to probe the angular distribution of the plasma charges, in the current paper the peculiar dynamics and energetics of various types of ions is finely investigated with the help of an Electrostatic Energy Analyzer (EEA). Only by using this EEA device (which was not available in the previous FC study [23]) can one separate, identify and deeply analyze the various ion classes (along with associated parameters as temperature, thermal and center-of-mass velocities etc.) through finely tuning the electrostatic fields between the EEA grids. This approach leads to detection of three distinct groups of ions. Their individual energy distributions (as well as global plasma parameters) are evaluated for various laser fluences and irradiation configurations.

By a multi-peak deconvolution procedure, the parameters characterizing each group of ions are derived.

2. Experimental details

The carbon plasma was generated by KrF excimer laser ablation of a pyrolytic graphite target in vacuum, for a residual gas pressure of 10^{-4} Pa (for a more detailed description of the experimental setup see also [23]). The 20 ns laser pulse with a typical beam profile (top-hat on the long axis, and approximately Gaussian on the short axis) was focused on the target at 45° incidence through a spherical lens of 50 cm focal distance, without additional optics for beam shaping or homogenizing. The laser fluence was varied in a low-moderate range (below 2.5 J/cm^2), either by changing the laser pulse energy while keeping constant the irradiated spot area of 0.2 cm^2, or by maintaining the same laser pulse energy while modifying the distance between the focusing lens and the target surface, further denoted by "lens position" (*LP*) [23,25].

Investigations of the positively charged carbon plasma species were carried out by using an electrostatic energy analyzer (Kimball Physics, FC-71A) placed at L = 17.5 cm along the normal to the target surface, without any additional adapters (drift tube or electrostatic mirrors). The EEA consists in three 5-mm diameter tungsten parallel grids of 64% open area (nettings of 20 μm diameter wires distanced at 200 μm), electrically isolated by 1 mm thickness ceramic rings, placed in the front of a Faraday cup (FC) – see the inset in Figure 1a. The EEA entrance grid is provided with an aperture of 5 mm diameter, to narrow the ion collecting area and to achieve a better spatial resolution, while a second aperture of 9.5 mm diameter is placed at the entrance of the FC. The total length of the device is much shorter than the distance to the target and consequently a one-dimensional plasma expansion model can be considered.

The first grid (GG), exposed directly to the plasma, is connected to ground to ensure a minimal electrical perturbation of the plasma. The second one, denoted as suppression grid (SG), is negatively biased at $V_{SG} = -9$ V, found to be enough for repelling the primary electrons arriving from the plasma. The third one, having the role of a retarding grid (RG), was positively biased in the range $V_{RG} = +(0 \div 120)$ V by using two stabilized power supplies (Hameg HM8143), to selectively repel ions of various energies. Finally, a voltage $V_{FC} = -9$ V applied on the FC was determined to be enough for repelling the possibly escaping primary electrons or the secondary electrons emitted by the interaction of plasma particles with the metallic grids (avoiding thus their interference with the recorded ion saturation current). In order to eliminate the artifacts in the electrical signal, batteries were used for passively biasing the collector and the SG. The electrical signals were recorded by using the 50 Ω input impedance of a 2 GHz oscilloscope (LeCroy), externally triggered by a fast photodiode (2 ns rise time) synchronized with the ablation laser pulse. Each recorded time-of-flight (TOF) signal was obtained as an average of ten laser shots directed onto fresh surfaces of the target, which was placed on an automated carousel.

3. Results and discussion

3.1. Global plasma parameters and their dependence on the laser fluence

In a first step, the laser fluence was varied by changing the pulse energy and keeping constant the ablation spot area of 0.2 cm^2 (LP=40 cm). The ion TOF signals recorded by the FC for the biasing scheme ($V_{SG} = -9$ V, $V_{RG} = 0$ V, $V_{FC} = -9$ V) are presented in Figure 1a as contour map obtained for various laser pulse energies. Typical examples for $E_L = 105$ mJ, $E_L = 135$ mJ, $E_L = 165$ mJ and $E_L = 200$ mJ are extracted in the upper graph, while the expected decrease of the signal amplitude with the decreasing of the energy is shown in the lateral plot.

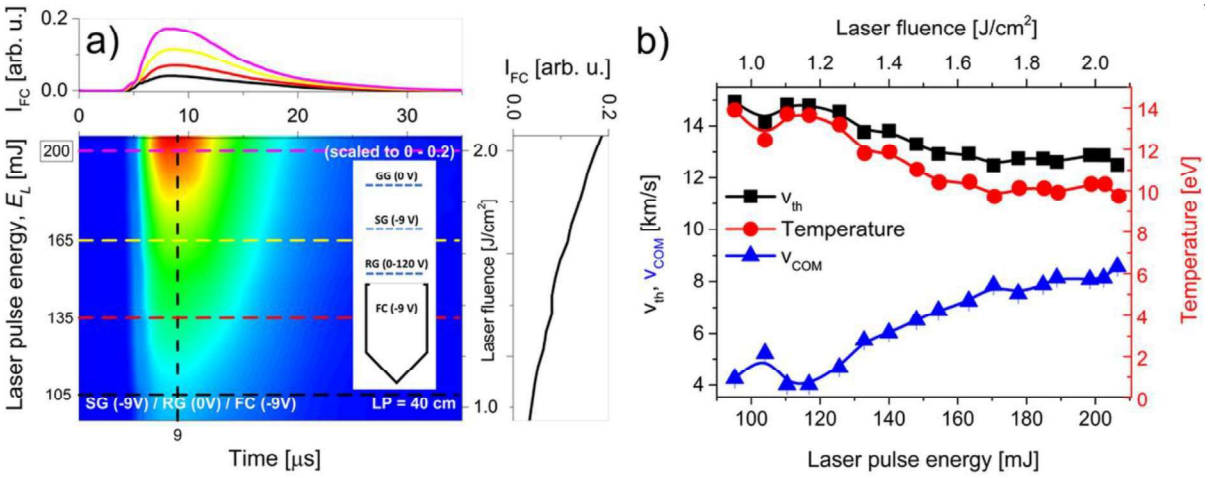

Figure 1 a) Contour map of TOF signals and b) derived global plasma parameters as functions of the laser pulse energy or fluence.

Rough estimations of the global plume parameters (temperature, center-of-mass and thermal velocities) can be obtained by fitting the recorded ion TOF curves with a single time-dependence resulted from the shifted Maxwell–Boltzmann (SMB) distribution [17]:

$$j(t) \propto t^{-n}\exp[-(L/t - v_{COM})^2/v_{th}^2] \quad (1)$$

where L is the total distance from the target to the ion collector, v_{COM} is the center-of-mass velocity and n a constant which depends on the collector geometry (area and distance from the target). The parameter $v_{th} = \sqrt{2k_B T_i/m}$ is the thermal velocity, related to the ion temperature, T_i, and mass, m. According to [17], the value of n is not influencing the order of magnitude of v_{COM} and v_{th} parameters, and similarly good fits, with comparable (high, >0.98) R^2 coefficients, are obtained for various values of n. We assumed here n=3, having in view the small diameter of the entrance aperture of the detection system (0.5 cm) when comparing with the target-FC distance (L = 17.5

cm), which avoids taking into account the velocity components parallel to the detector surface [27–29].

In Figure 1a we observe that the moment at which the ion current reaches its maximum remains almost constant, at about $t_{max} \cong 9\ \mu s$, regardless of the laser pulse energy. Theoretically, from Eq. (1) in general form, t_{max} can be derived as,

$$t_{max} = \frac{L}{n \cdot v_{th}} \left(-w + \sqrt{w^2 + 2n}\right), \tag{2}$$

where w is the ratio between the center-of-mass and thermal velocities, $w = v_{COM}/v_{th}$. The fitting of our data with Eq. (1) returns values of w much lower than unity, and thus according with Eq. (2) t_{max} is mainly influenced by v_{th}. Indeed, as plotted in Figure 1b, the resulting thermal velocity (and implicitly the effective temperature associated with the translational motion along the plume axis [30]), is only slowly depending on the laser pulse energy, displaying a decreasing trend, from ~14 km/s to ~12 km/s. The center-of-mass velocity shows the opposite behavior: it significantly increases from 4 km/s to almost the double when the laser pulse energy is doubled (see Figure 1b). We note that some minor deviations from a monotonic dependence can probably be ascribed to ablation laser fluctuations.

Similar estimations were previously reported in Figure 8 of [23], but for constant laser energy, E_L = 264 mJ (higher than in the present experiments), and increasing the laser fluence from 1.2 J/cm^2 to 2.1 J/cm^2 in a different manner: by varying the *LP* between 41 cm and 46 cm to change the spot area. The FC was placed closer to the target, at L = 14 cm, but such difference is not relevant when regarding the plasma evolution. In contrast with the present measurement, we found there a noticeable decrease of t_{max} in the TOF profiles. Correspondingly, that was given by a significant increase of the thermal velocity from 6 km/s, followed by a saturation trend at about 14

km/s. Meantime, the center-of-mass velocity was almost constant, v_{COM} = 12 km/s at low fluences, with a slight increase to v_{COM}=14 km/s for *LP*=46 mm.

For comparing the results from [23] with the present ones (Figure 1b), extrapolations are required toward the above mentioned higher energy of the laser pulse, E_L = 264 mJ, and correspondingly toward higher fluences. For sake of simplicity, the dependences were considered as linear, and thus one can estimate $v_{COM} \cong$ 11 km/s and $T \cong$ 10 eV. Such results are in reasonable agreement with the previous ones from [23], having in view the slightly different detection distance used in the present measurements.

A possible explanation for the plasma temperature decrease with the laser fluence (Figure 1b), in the context of the center-of-mass velocity and signal amplitude increase, can be related to the increase of the ablated mass, resulting in the screening of the laser beam by plasma absorption, which further contributes to plasma heterogeneity (some parts of it becoming hotter, see Figure 6). We also assume a possible influence of the laser energy distribution on the spot area, that previously led to an unusual V-shape light emitting plasma (found connected with crater geometry [23]). Therefore, we conclude that, when such a laser type of rectangular spot is used, the way how the laser fluence is adjusted (through the spot area by changing the focusing lens position or through the laser pulse energy changing) significantly influences the plasma parameters. Alternatively, one can simply agree with [30], where the meaning of the SMB fitting parameters was found to be questionable when accelerated ions significantly contribute to the TOF measured signal. In our opinion, such discussion is valid for the derived effective temperatures, whereas the center-of-mass velocities are fitting well the one resulted from the optical measurements [23].

3.2. Charge separation in the retarding electric field, correlation with the suppression grid signal and ion energy distribution

Let us now observe the influence of the positive bias V_{RG} (applied on the retarding grid) on the FC signal, in the biasing scheme V_{SG} = –9 V, V_{RG} = +(0÷120) V, V_{FC} = –9 V. This is presented in Figure 2a-c as contour maps obtained from the TOF signals recorded at various RG voltages, for E_L = 288 mJ and different lens positions, *LP* = 40 cm - a), *LP* = 42 cm - b) and *LP* = 45 cm - c), which correspond to laser fluences of 1.1 J/cm^2, 1.26 J/cm^2, and 1.66 J/cm^2, respectively. We mention that in the followings we aim to observe the influence of the laser beam focusing conditions on the ions production, and not the role of the laser pulse energy, as studied in the previous paragraph.

The typical shapes of the FC signals are extracted in the upper plots for some selected V_{RG} (see the corresponding dotted lines on the contour maps). One can easily notice the occurrence of multiple peaks in the TOF profiles, *i.e.* the separation of various populations of ions by the retarding electric field. Taking into account our previous spectroscopic studies [23], these species are straightforwardly assigned to the C^{2+} and C^{1+}_{fast} ions in the "fast" plasma structure evidenced by optical investigations. The C^{1+}_{slow} ions can be found in the "slow" plasma structure [26], which results here in a hump on the tail of the TOF profile. One can also infer a characteristic time for the maximum of each peak (see the vertical dotted lines in Figures 2a-c) that is significantly influenced by the *LP* focusing conditions, *i.e.* by the laser fluence. For example, in the case of C^{2+} ion group, it decreases in average from 9 μs for *LP* = 40 cm to 6 μs for *LP* = 45 cm, while for C^{1+}_{fast} from 14 μs to 8.6 μs. Having in view the discussion from Section 3.1 (regarding the estimations previously reported in Figure 8 of [23]), these decreases can be easily explained by the increase of the plasma thermal velocity, *i.e.* of the effective plasma temperature, with the laser fluence.

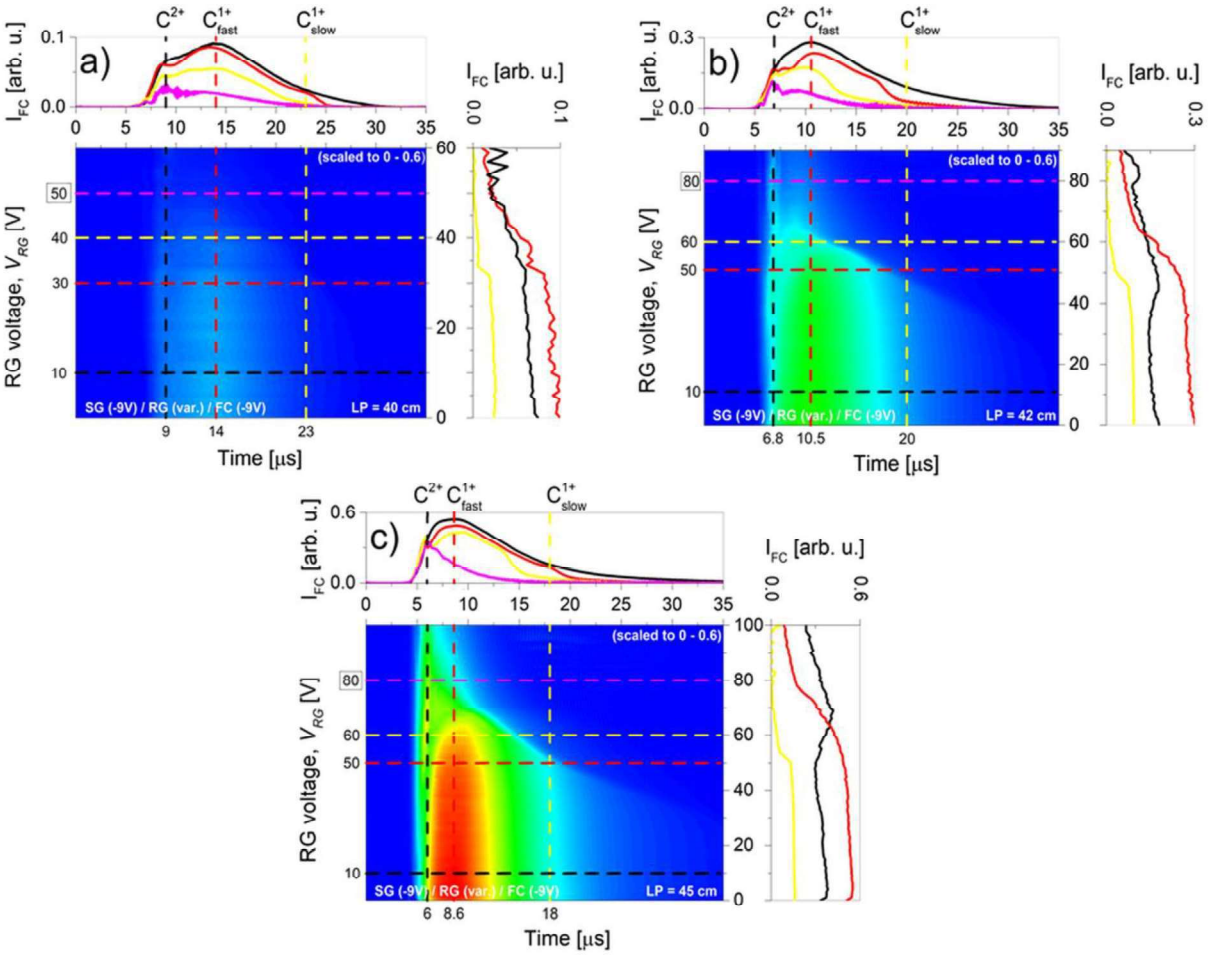

Figure 2 Contour maps derived from TOF profiles obtained for E_L = 288 mJ and different focusing conditions: a) LP=40 cm, b) LP=42 cm, and c) LP=45 cm.

Through a more detailed analysis, we observed that the amplitudes (maxima of the ion current) and the times required for specific ion groups to reach their maximum are influenced by the retarding grid voltage as well. In Figure 3a-c, the dependences of these parameters on the V_{RG} voltage were extracted from the temporal traces given above. Depending on their kinetic energy, the ions are progressively repelled and decelerated, and subsequently the peaks amplitude is decreasing, while the corresponding time of maximum is increasing, regardless to the laser beam focusing conditions.

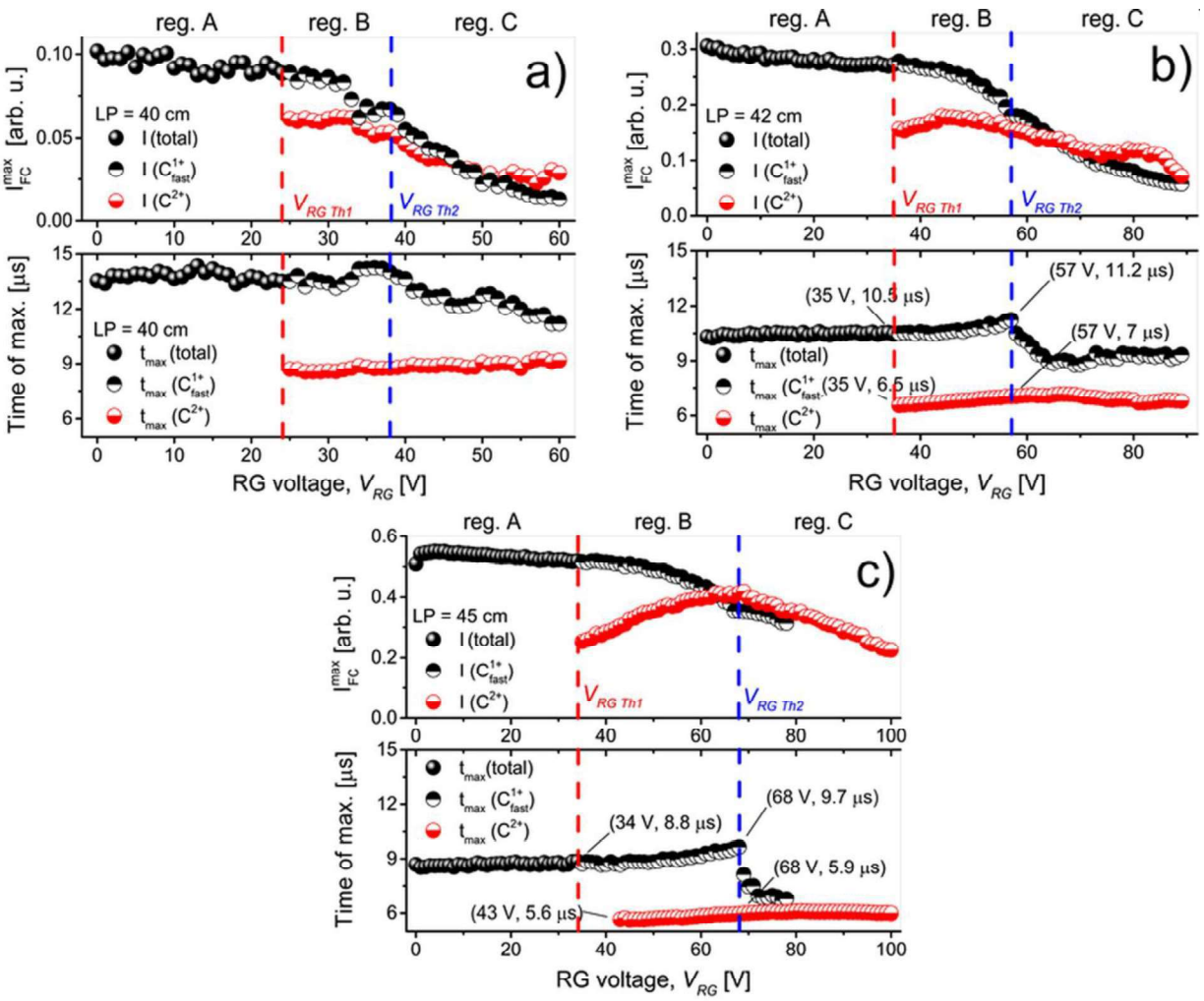

Figure 3 EEA-FC recorded maximum ion current and the corresponding time values as a function of RG bias for various lens positions: a) *LP* = 40 cm, b) *LP* = 42 cm and c) *LP* = 45 cm.

At low V_{RG} voltages, the EEA-FC signal has a single-peak structure, of slowly decreasing amplitude (A region in Figure 3, in correspondence with the temporal traces from Figure 2). Then, it splits in two peaks (B region), at a threshold value $V_{RG\ Th1}$ (that is *LP* dependent - see the dotted red lines in Figure 3). A main peak of decreasing amplitude is determined by the C^{1+}_{fast} ions. It is continuing the evolution from the single-peak structure, showing thus the higher abundance of this ion. A second peak is given by the C^{2+} ions, being suddenly evidenced at earlier times when

increasing the V_{RG} voltages. It has at the beginning a peculiar behavior due to the amplitude increase for a certain V_{RG} range, followed by the expected decreasing trend. Both ions belong to the fast plasma structure, and such unusual initial amplitude increasing of the second peak is possibly explained by the charges decoupling process. This is influenced by various factors: collisions between different types of plasma particles, complex space distribution of the electrostatic retarding field and its shielding by space charge structures, subsequent incomplete suppression of electrons by the SG. Moreover, having in view that the expanding plasma parameters are also space- and time-dependent, a complete description of the charge separation process is difficult to be achieved. Therefore, effective values of the grid potentials and transparency coefficients should be considered when operating with exact energetic values (see below).

The separation process ends at a second threshold $V_{RG\ Th2}$ (see dashed blue lines), which determines the C-region in Figure 3. Starting with this value, the TOF signals amplitudes continue their descendant evolution while the time maximum of C^{1+}_{fast} peak rapidly decreases toward a constant value, because the C^{1+}_{fast} ion group is almost completely repelled. The electric potential $V_{RG\ Th2}$ is roughly seen here at the first glance to depend on the focusing conditions, *i.e.* on the laser fluence, and therefore on the ion kinetic energy, as it will be detailed below.

To extract the plasma parameters from the experimental data obtained using the retarding field energy analyzer, by time-integration of the EEA-FC signal, we built the collector characteristics, *i.e.* the dependences of the total collected charge *vs.* the retarding potential. In Figure 4a) they are given for the previous *LP*s, showing as expected the increase of the charge production with the laser fluence, and the diminishing of the collected charge with the RG voltage. Then, following the interpretation from [31], the derivative was calculated to obtain the energy distribution function given in Figure 4b, for the direction parallel to the plume axis. One observes a good agreement of fitting with the SMB distribution function written in the form [31]:

$$f(V_{RG}) = C \cdot exp\left[-\left(\sqrt{eV_{RG}} - \sqrt{eV_{RG-COM}}\right)^2 / E_{th}\right] \quad (3)$$

where C is a constant, V_{RG-COM} is the potential corresponding to the kinetic energy associated with the center-of-mass velocity, $V_{RG-COM} = mv_{COM}^2/2e$, and E_{th} the associated thermal energy. It results the fitting parameters $eV_{RG-COM} = (38.4 \pm 0.4;\ 54.7 \pm 0.2;\ 62.3 \pm 0.2)\ eV$ and $E_{th} = (1.08 \pm 0.15;\ 0.99 \pm 0.05;\ 1.18 \pm 0.05)\ eV$ for $LP = (40; 42; 45)$ cm, respectively. We note an excellent agreement of V_{RG-COM} values with the previous ones of $V_{RG\ Th2}$, but deduced through a different manner. This result infers that the ion separation process in the fast plasma structure ends at the potential corresponding to the maximum of SMB distribution function.

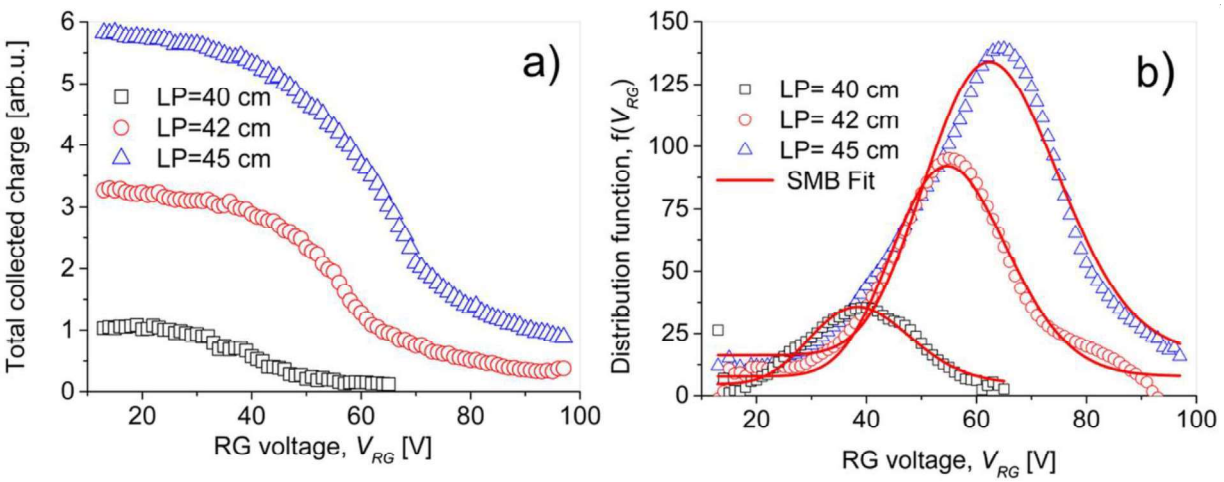

Figure 4 a) Total collected charge - RG bias characteristics and b) ion energy distribution functions for various lens positions.

One should also note that the values of eV_{RG-COM} and E_{th}, resulted from the numerical fitting in Figure 3b, are much different when comparing with those that could be estimated from the velocities of the order $10^3 \div 10^4\ m/s$ and the previous temperatures (see Figure 1b). In our opinion this discrepancy is given by the requirement of considering a transparency coefficient of the RG, having in view that the grid transparency is influencing the absolute value of the collector

current. Thus, the corresponding coefficient should correct the retarding field to an effective (real) value, which is imposed by the complex space-distribution of the electrical field produced by the RG and its possible shielding effects. Therefore, in the absence of initial calibration of our EEA using a completely characterized ion source, instead of absolute values we can only remark here the good agreement with the SMB distribution function and suggest future possible developments of such a derivative method which is usually applied for stationary plasmas [32].

3.3. Ion abundance and the dependence on laser pulse energy

According with the previous section, at the retarding voltage V_{RG} = +90 V, the charge separation process is completely accomplished, and the temporal trace of the ion collector presents two peaks. They correspond to C^{2+} and C^{1+}_{fast} ions from the fast plasma part and are followed by a hump which is assigned to C^{1+}_{slow} ion from the slow part. We further preserve the tight focus of the laser beam, by using a focusing distance LP = 46 cm, and the biasing scheme (V_{SG} = –9 V, V_{RG} = +90 V, V_{FC} = –9 V). The laser fluence is varied by changing the pulse energy, similarly to Section 3.1. The aim of the present measurements is to individually investigate the production of different types of ions, *i.e.* their abundance and their expansion parameters. In Figure 5a we first use a contour map to present the EEA-FC signal, having the typical shapes shown in the upper plot for certain values of the laser pulse energy (see the corresponding dotted lines). The right-side graph of Figure 5a displays the expected signal amplitude increase with the laser pulse energy for several temporal instances.

To get more insights on the plasma species content, we further performed a numerical fitting of the data, by considering an overlapping of three time-dependences derived from the SMB

distribution. According with Eq. (1) and using the parameters specified from Eq. (2), the current density was taken in the form:

$$j(t) = \sum_i A_i \cdot t^{-3} \exp\left[-\left((L/t)/v_{t\square,i} - w_i\right)^2\right], \quad (4)$$

with A the amplitude and i the index specifying the ion type. The only fixed and common parameter was considered the target-collector distance, L. Leaving free the A_i parameters, together with $v_{t\square,i}$ and w_i, no additional measurement of ion abundance is required, as in [18]. However, the present method is restricted to only a few types of ions, due to the potential high number of parameters to be computed.

In Figure 5b, such type of fitting is presented as example, for the laser pulse energy of E_L = 206 mJ (LP = 46 cm), and it shows that most of the collector signal is given by the fast plasma part. The slow plasma structure, which is present in the tail of the EEA-FC signal, consists mostly in singly charged ions and probably neutrals. We observe again that the returned w_i ratios are much lower than unity, which allows us to neglect them in (4). Then, having in view the same interpretation as in Section 3.1, the value of t_{max} is mainly imposed by v_{th}, and therefore the temperature characterizing each type of ion can be simply estimated, as shown below.

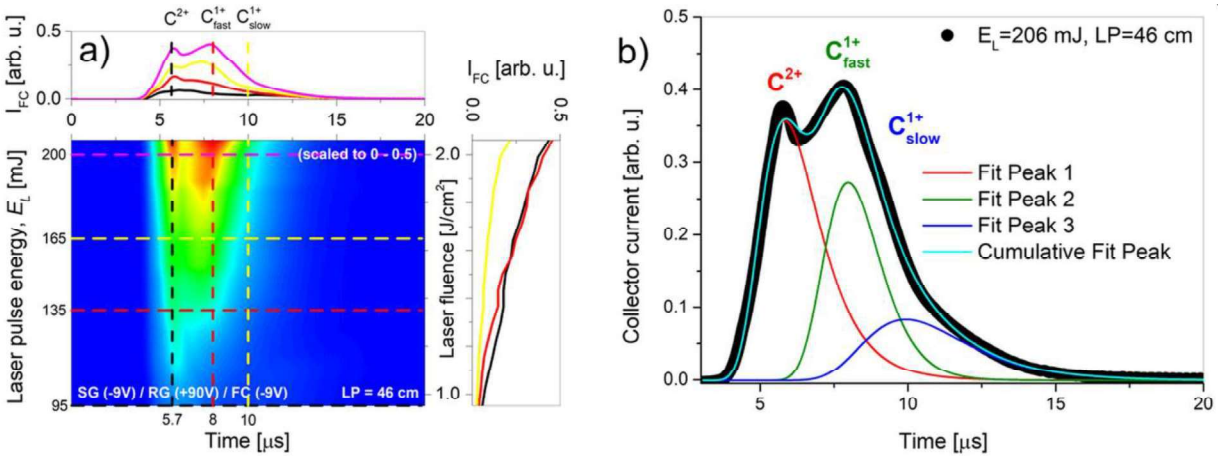

Figure 5 a) Contour map of the TOF signal for the biasing scheme (V_{SG} = –9 V, V_{RG} = +90 V, V_{FC} = –9 V), at various laser pulse energies (LP = 46 cm), and b) typical example of SMB numerical fitting.

Using the present experimental data, the fitting procedures succeeded with a good accuracy only for the highest laser pulse energies considered in the experiments, *i.e.* only for high fluences, when the peak of each ion group is clearly distinguished. To further simplify and to extend our interpretations, the w_i ratio is neglected in Eqs. (2) and (4), since values much lower than unity were obtained. This allows accurate deduction of only two parameters: the amplitude A_i and the time $t_{max,i}$ of the maximum current, specific for each ion type i. This assumption reduced the fitting procedure to compute in total six independent parameters and the base line. The dependences of the resulting plasma parameters on the laser pulse energy are plotted in Figure 6. One observes a significant increase of C^{2+} and C^{1+}_{fast} ions production with the laser pulse energy, while the amount of singly charged ions in the thermal plasma part is less affected (Figure 6a). Also, since the times of maximum current of each type of ion has only low fluctuations (Figure 5a), probably given by the accuracy of the fitting procedure, the same limited variation is found for the thermal velocity and implicitly for the temperature. This last result agrees with Section 3.1 where, even at lower laser fluences (LP = 40 cm), no significant shift of the time corresponding to the maximum ion current was revealed when varying the laser pulse energy (Figure 1a).

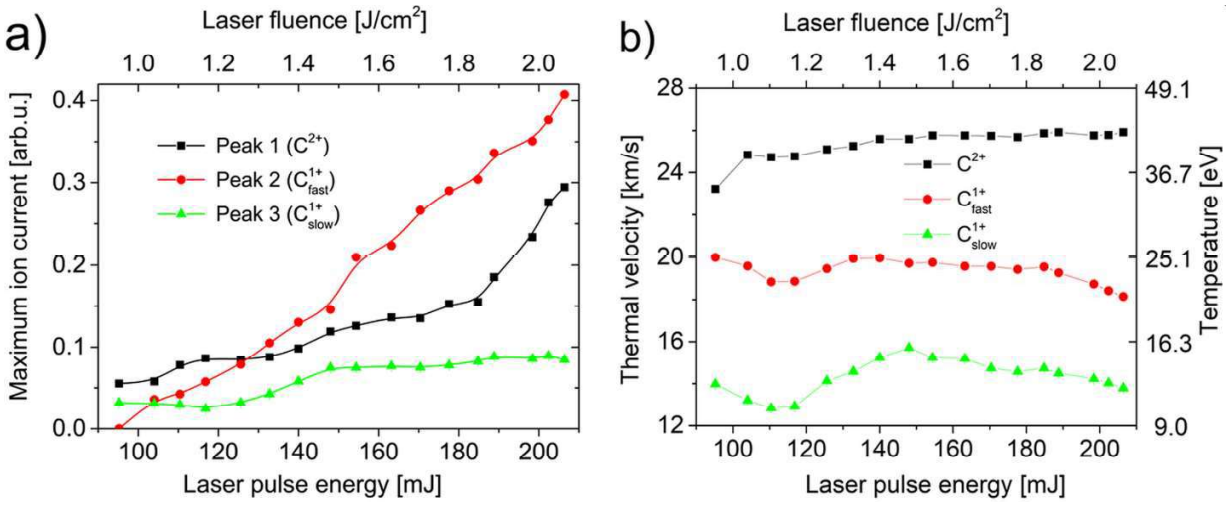

Figure 6 Laser pulse energy effect on a) the ion current amplitude and b) the thermal velocity for the three types of ions.

According to the previous considerations, t_{max} is mainly determined by the thermal velocity (or by the equivalent temperature). When averaging for all laser pulse energies, one obtains thermal energies of ~42 eV for C^{2+}, ~23 eV for C^{1+}_{fast} and ~13 eV for C^{1+}_{slow}, *i.e.* in reasonable agreement as order of magnitude with the previous values from Figure 1b, having in view that such global values were obtained for lower fluences. We note also that for all these estimations the value n=3 was considered in Eq. (2), and rescaling is possible if one considers a different n value.

4. Conclusions

A transient carbon plasma produced by KrF excimer laser ablation at moderate fluences was electrically investigated with an electrostatic energy analyzer to characterize the ion energetics, having in mind possible applications in the PLD field. The laser fluence variation was achieved in two distinct manners: either by varying the pulse energy while keeping constant the irradiation spot size, or, reversely, by changing the focusing lens – target distance while keeping the laser pulse

energy constant. Although equivalent at first sight, we emphasize here that these two approaches can in fact be quite different. Indeed, the reported fluence values are actually averaged over the entire irradiated spot surface, but the "local" fluence values can span a wide range (see, e.g., Figure 1 of [23]). Moreover, changing the focusing of a rectangular beam changes the shape of the intensity distribution function, possibly leading to high intensities along the longer beam axis for tight focusing. The two approaches must therefore be considered separately (one example is the different behavior of the time needed for reaching maximum ion current in the two approaches).

By using the repelling electric field in the EEA, it was possible to unveil the multi-peak structure of the recorded ion current and to assign the observed individual components to distinct types of ions and plasma structures. By time-integrating of EEA-FC signal, the dependence of the total collected charge on the retarding grid potential was plotted, leading to the derivation of energy distribution functions in good agreement with the SMB distribution. From the SMB fitting, the center-of-mass velocity showed a pronounced dependence on the laser fluence, while the thermal velocity displayed a much narrower evolution. Finally, the influence of the laser pulse energy on the production of different types of ions was studied by using a multi-peak fitting procedure. A significant increase of C^{2+} and C^{1+}_{fast} ions production with the pulse energy was observed, while the amount of singly charged ion in the slower plasma structure was less affected by the irradiation conditions.

In conclusion, by using a simple EEA it is possible to discern between different types of ions and structures contained in the laser produced plasma. The numerical fitting of the signal with a time-dependence derived from the shifted Maxwell-Boltzmann distribution allows estimation of the relative abundances and of the thermal velocities. Further developments of this method are possible by accommodating the experimental results with theoretical calculations of fractional

populations obtained through different plasma models, such as local thermodynamic equilibrium, collisional-radiative, or corona [33], and this will be subjected to future work.

Acknowledgments

Part of this work was supported by the French National Research Agency (ANR) under contracts ANR-18-CE22-0019 (UNREAL) and ANR-10-LABX-005 (LABEX CaPPA).

References

[1] J.D. Gillaspy, Highly charged ions, J. Phys. B At. Mol. Opt. Phys. 34 (2001). https://doi.org/10.1088/0953-4075/34/19/201.

[2] F. Aumayr, H. Winter, Potential sputtering, Philos. Trans. R. Soc. A Math. Phys. Eng. Sci. 362 (2004) 77–102. https://doi.org/10.1098/rsta.2003.1300.

[3] R. Eason (Ed.), Pulsed laser deposition of thin films: applications-led growth of functional materials, John Wiley & Sons, Hoboken, New Jersey, 2007.

[4] H. Krebs, M. Störmer, S. Fähler, O. Bremert, M. Hamp, A. Pundt, H. Teichler, W. Blum, T. Metzger, Structural properties of laser deposited metallic alloys and multilayers, Appl. Surf. Sci. 109–110 (1997) 563–569. https://doi.org/10.1016/S0169-4332(96)00635-6.

[5] H. Ullmaier, Radiation damage in metallic materials, MRS Bull. 22 (1997) 14–21. https://doi.org/10.1557/S088376940003298X.

[6] H. Windischmann, An intrinsic stress scaling law for polycrystalline thin films prepared by ion beam sputtering, J. Appl. Phys. 62 (1987) 1800–1807. https://doi.org/10.1063/1.339560.

[7] J.A. Thornton, D.W. Hoffman, Stress-related effects in thin films, Thin Solid Films 171 (1989) 5–31. https://doi.org/10.1016/0040-6090(89)90030-8.

[8] Y. Yamagata, A. Sharma, J. Narayan, R.M. Mayo, J.W. Newman, K. Ebihara, Optical

emission study of ablation plasma plume in the preparation of diamond-like carbon films by KrF excimer laser, J. Appl. Phys. 86 (1999) 4154–4159. https://doi.org/10.1063/1.371340.

[9] A.A. Puretzky, D.B. Geohegan, X. Fan, S.J. Pennycook, Dynamics of single-wall carbon nanotube synthesis by laser vaporization, Appl. Phys. A Mater. Sci. Process. 70 (2000) 153–160. https://doi.org/10.1007/s003390050027.

[10] A.A. Puretzky, H. Schittenhelm, X. Fan, M.J. Lance, L.F. Allard, D.B. Geohegan, Investigations of single-wall carbon nanotube growth by time-restricted laser vaporization, Phys. Rev. B. 65 (2002) 245425. https://doi.org/10.1103/PhysRevB.65.245425.

[11] C.-C. Moise, M. Enachescu, High-quality carbon nanomaterials synthesized by excimer laser ablation, in: Appl. Laser Ablation - Thin Film Depos. Nanomater. Synth. Surf. Modif., InTech, 2016: p. 13. https://doi.org/10.5772/65309.

[12] D. Doria, A. Lorusso, F. Belloni, V. Nassisi, L. Torrisi, S. Gammino, A study of the parameters of particles ejected from a laser plasma, Laser Part. Beams. 22 (2004) 461–467. https://doi.org/10.1017/S0263034604040108.

[13] J. Krása, K. Jungwirth, S. Gammino, E. Krouský, L. Láska, A. Lorusso, V. Nassisi, M. Pfeifer, K. Rohlena, L. Torrisi, J. Ullschmied, A. Velyhan, Partial currents of ion species in an expanding laser-created plasma, Vacuum 83 (2008) 180–184. https://doi.org/10.1016/j.vacuum.2008.03.031.

[14] O. Balki, H.E. Elsayed-Ali, Multicharged carbon ion generation from laser plasma, Rev. Sci. Instrum. 87 (2016) 113304. https://doi.org/10.1063/1.4966987.

[15] M.H.A. Shaim, F.G. Wilson, H.E. Elsayed-Ali, Aluminum multicharged ion generation from femtosecond laser plasma, J. Appl. Phys. 121 (2017) 185901. https://doi.org/10.1063/1.4983008.

[16] M.H.A. Shaim, H.E. Elsayed-Ali, Characterization of laser-generated aluminum plasma

using ion time-of-flight and optical emission spectroscopy, J. Appl. Phys. 122 (2017) 203301. https://doi.org/10.1063/1.4995477.

[17] P. Nica, S. Gurlui, M. Osiac, M. Agop, M. Ziskind, C. Focsa, Investigation of femtosecond laser-produced plasma from various metallic targets using the Langmuir probe characteristic, Phys. Plasmas. 24 (2017) 103119. https://doi.org/10.1063/1.5006076.

[18] M.H.A. Shaim, H.E. Elsayed-Ali, Aluminum multicharged ion generation from laser plasma, Nucl. Instrum. Methods Phys. Res., Sect. B 356–357 (2015) 75–80. https://doi.org/10.1016/j.nimb.2015.04.066.

[19] M.H.A. Shaim, F.G. Wilson, H.E. Elsayed-Ali, Aluminum multicharged ion generation from femtosecond laser plasma, J. Appl. Phys. 121 (2017) 185901. https://doi.org/10.1063/1.4983008.

[20] C. Focsa, S. Gurlui, P. Nica, M. Agop, M. Ziskind, Plume splitting and oscillatory behavior in transient plasmas generated by high-fluence laser ablation in vacuum, Appl. Surf. Sci. 424 (2017) 299–309. https://doi.org/10.1016/j.apsusc.2017.03.273.

[21] C. Ursu, P.-E. Nica, Diagnosis of carbon laser produced plasma by using an electrostatic energy analyzer, J. Optoelectron. Adv. Mater. 15 (2013) 42–45.

[22] P.-E. Nica, G.B. Rusu, O.-G. Dragos, C. Ursu, Effect of excimer laser beam spot size on carbon laser-produced plasma dynamics, IEEE Trans. Plasma Sci. 42 (2014) 2694–2695. https://doi.org/10.1109/TPS.2014.2350532.

[23] C. Ursu, P. Nica, C. Focsa, Excimer laser ablation of graphite: The enhancement of carbon dimer formation, Appl. Surf. Sci. 456 (2018) 717–725. https://doi.org/10.1016/j.apsusc.2018.06.217.

[24] M. Agop, P.E. Nica, S. Gurlui, C. Focsa, V.P. Paun, M. Colotin, Implications of an extended fractal hydrodynamic model, Eur. Phys. J. D. 56 (2010) 405–419.

https://doi.org/10.1140/epjd/e2009-00304-5.

[25] C. Ursu, P. Nica, C. Focsa, M. Agop, Fractal method for modeling the peculiar dynamics of transient carbon plasma generated by excimer laser ablation in vacuum, Complexity. 2018 (2018) 1–8. https://doi.org/10.1155/2018/1814082.

[26] C. Ursu, P. Nica, B.G.G. Rusu, C. Focsa, V-shape plasma generated by excimer laser ablation of graphite in argon: Spectroscopic investigations, Spectrochim. Acta, Part B 163 (2020) 105743. https://doi.org/10.1016/j.sab.2019.105743.

[27] R. Kelly, R.W. Dreyfus, On the effect of Knudsen-layer formation on studies of vaporization, sputtering, and desorption, Surf. Sci. 198 (1988) 263–276. https://doi.org/10.1016/0039-6028(88)90483-9.

[28] J. Krása, A. Lorusso, D. Doria, F. Belloni, V. Nassisi, K. Rohlena, Time-of-flight profile of multiply-charged ion currents produced by a pulse laser, Plasma Phys. Controlled Fusion 47 (2005) 1339–1349. https://doi.org/10.1088/0741-3335/47/8/012.

[29] D. Doria, A. Lorusso, F. Belloni, V. Nassisi, Characterization of a nonequilibrium XeCl laser-plasma by a movable Faraday cup, Rev. Sci. Instrum. 75 (2004) 387–392. https://doi.org/10.1063/1.1641157.

[30] N.M. Bulgakova, A. V. Bulgakov, O.F. Bobrenok, Double layer effects in laser-ablation plasma plumes, Phys. Rev. E: Stat. Phys. Plasmas Fluids Relat. Interdiscip. Top. 62 (2000) 5624–5635. https://doi.org/10.1103/PhysRevE.62.5624.

[31] H.M. Küdyan, Interpretation of electrostatic energy analyzer data of a flowing plamsa, Rev. Sci. Instrum. 49 (1978) 8–10. https://doi.org/10.1063/1.1135262.

[32] W. Lochte-Holtgreven, Plasma Diagnostics, Cambridge International Science Publishing, Cambridge, 2005. http://www.osti.gov/energycitations/product.biblio.jsp?osti_id=4798641.

[33] David Salzmann, Atomic physics in hot plasmas, Oxford University Press, Oxford, 1998.